Curvature sensing of curvature-inducing proteins with internal structure

Hiroshi Noguchi *

Institute for Solid State Physics, University of Tokyo, Kashiwa, Chiba 277-8581, Japan

(Received 4 September 2023; accepted 15 January 2024; published 7 February 2024)

Many types of peripheral and transmembrane proteins can sense and generate membrane curvature. Laterally isotropic proteins and crescent proteins with twofold rotational symmetry, such as Bin/Amphiphysin/Rvs superfamily proteins, have been studied theoretically. However, proteins often have an asymmetric structure or a higher rotational symmetry. We studied theoretically the curvature sensing of proteins with asymmetric structures and structural deformations. First, we examined proteins consisting of two rodlike segments. When proteins have mirror symmetry, their sensing ability is similar to that of single-rod proteins; hence, with increasing protein density on a cylindrical membrane tube, a second- or first-order transition occurs at a middle or small tube radius, respectively. As asymmetry is introduced, this transition becomes a continuous change and metastable states appear at high protein densities. Protein with threefold, fivefold, or higher rotational symmetry has laterally isotropic bending energy. However, when a structural deformation is allowed, the protein can have a preferred orientation and stronger curvature sensing.

DOI: 10.1103/PhysRevE.109.024403

I. INTRODUCTION

In living cells, biomembranes are primarily composed of lipids and proteins. Transmembrane proteins span the membrane, while peripheral proteins bind and unbind to the membrane surface. Many of these proteins modify membrane properties, such as bending rigidity, spontaneous curvature, membrane thickness, and viscosity. Curvature-inducing proteins, such as the Bin/Amphiphysin/Rvs (BAR) superfamily of proteins, regulate cell and organelle membrane shapes [1,2]. The BAR superfamily proteins have a crescent binding domain (BAR domain), which is a dimer with twofold rotational symmetry. The BAR domain bends membranes along its axis and generates a cylindrical membrane tube [1–7]. Clathrin and coat protein molecules assemble to form spherical cargo, generating spherical membrane buds [3,8–12]. These curvature-inducing proteins sense membrane curvature and are concentrated at the membrane locations of their preferred curvatures. Curvature sensing of BAR proteins [13–17], dynamin [18], annexins [19], G-protein coupled receptors (GPCRs) [20], ion channels [21,22], and Ras proteins [23] has been reported using tethered vesicles. The dependence of protein binding on vesicle size also indicates curvature sensing [23–25].

Theoretically, curvature-inducing proteins have been modeled as laterally isotropic or crescent objects. For isotropic objects, the Canham-Helfrich model [26,27] was applied to the bending energy [16,17,28–31]. For crescent objects, anisotropic bending energies were considered [28,32–37]. An elliptical shape was typically considered, such that a twofold rotational and mirror-symmetric shape was assumed. However, actual proteins often have more complicated shapes. BAR domains have twofold rotational symmetry but are chiral and are not mirror symmetric [see Fig. 1(b)]. Their chirality is the origin of the helical assembly of the BAR domains [6,7] and is important for generating membrane tubes with a constant radius [38]. Many BAR and other curvature-inducing proteins have intrinsically disordered domains [39], and recent experiments have demonstrated that these disordered domains have significant effects on curvature generation [25,40,41]. Theoretically, they are treated as excluded-volume linear polymer chains. At a low polymer density on the membrane surface, polymer-membrane interactions can weakly induce a spontaneous curvature in a laterally isotropic manner [42–46]. Conversely, at high densities, interpolymer interactions can induce a large spontaneous curvature [42,46–49] and promote membrane tubulation or prevent it because of the repulsion between polymers [50].

In this study we consider two types of curvature-inducing proteins: asymmetric proteins and proteins with threefold or higher rotational symmetry (see Fig. 1). Dynamin [51–53] has an asymmetric structure and its helical assembly induces membrane fission by choking a membrane neck. Melittin and amphipathic peptides [54–57] bind onto the membrane and their circular assembly forms a membrane pore. Gómez-Llobregat *et al.* reported the curvature sensing of three amphipathic peptides using a coarse-grained simulation of a buckled membrane [58]. They revealed that melittin and the amphipathic peptides LL-37 (PDB: 2k6O) exhibited asymmetric curvature sensing, which means the angle distribution with respect to the buckled axis was not symmetric. We use a protein model consisting of two crescent-rodlike segments connected by a kink, like melittin [see Fig. 2(a)], and investigate how the asymmetry modifies curvature sensing.

Many transmembrane proteins, such as ion channels [59,60] and GPCRs [61–64], form rotational symmetric structures. Several types of microbial rhodopsins form a trimer

* noguchi@issp.u-tokyo.ac.jp

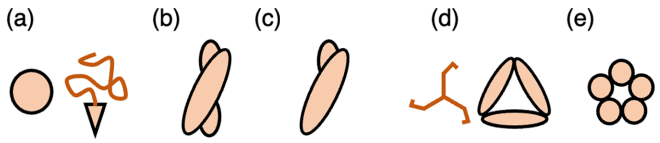

FIG. 1. Lateral symmetries of proteins on a membrane. (a) Laterally isotropic proteins, modeled as a circular shape on the membrane. Intrinsically disordered protein (IDP) domains and the insertion of a hydrophobic α helix can bend the membrane isotropically. (b) Twofold rotational symmetry. BAR superfamily proteins form a dimer that has twofold symmetry. (c) Asymmetric proteins. Dynamin and amphipathic peptides such as melittin do not have rotational symmetry. (d) Threefold rotational symmetry. The clathrin monomer has a threefold symmetric shape (left image). The trimers of proteins such as annexin and microbial rhodopsins also have threefold symmetry (right image). (e) Fivefold rotational symmetry. Transmembrane proteins, such as ion channels, and their assemblies often have fivefold or higher symmetries.

or pentamer with threefold or fivefold symmetry, respectively [64]. Moreover, peripheral proteins can have threefold symmetry. For example, the clathrin monomer has threefold symmetry [8] and annexin A5 molecules form a trimer with a triangular shape [65,66]. Recently, deformation of the lipid bilayer induced by the hydrophobic mismatch of rotationally symmetric transmembrane proteins was studied theoretically [67]. In this study we investigate curvature sensing of N-fold rotationally symmetric proteins with $N \geqslant 3$. The rigid rotationally symmetric proteins exhibit isotropic bending energy. However, the anisotropy can be induced by protein deformation.

The paper is structured as follows. The previous theoretical models of curvature-inducing proteins are outlined in Sec. II. The curvature sensing of asymmetric proteins is described in Sec. III. The protein model is presented in Sec. III A. Curvature sensing at low-density limits and at finite densities is described in Secs. III B and III C, respectively. Section IV discusses proteins with threefold or higher rotational symmetries. Section V summarizes the paper.

II. PROTEIN MODELS WITH ANISOTROPIC BENDING ENERGY

Crescent proteins were modeled to have different bending rigidities and spontaneous curvatures along the protein axis and in the perpendicular (side) direction. Note that this protein axis is set along the main preferred curvature of the protein on the membrane so that it can be different from the protein axis of the elliptical approximation (e.g., BAR-PH domains [5,6]). The membrane curvatures along these two directions are given by

$$C_{\ell 1} = C_1 \cos^2(\theta_{\rm pc}) + C_2 \sin^2(\theta_{\rm pc}) = H + D\cos(2\theta_{\rm pc}), \quad (1)$$

$$C_{\ell 2} = C_1 \sin^2(\theta_{\rm pc}) + C_2 \cos^2(\theta_{\rm pc}) = H - D\cos(2\theta_{\rm pc}), \quad (2)$$

where $\theta_{\rm pc}$ is the angle between the protein axis and the direction of either principal membrane curvature [the azimuthal direction is chosen for a cylindrical membrane as depicted in Fig. 2(b)], $H = (C_1 + C_2)/2$ and $D = (C_1 - C_2)/2$ represent the mean and deviatoric curvatures of the membrane, respectively, and C_1 and C_2 represent the principal curvatures. The bending energy of a protein is expressed as [28,36,68]

$$\begin{aligned} U_{\rm 1rod} &= \frac{\kappa_{\rm p} a_{\rm p}}{2}(C_{\ell 1} - C_{\rm p})^2 + \frac{\kappa_{\rm s} a_{\rm p}}{2}(C_{\ell 2} - C_{\rm s})^2 \quad (3)\\ &= a_{\rm p}\Bigg[\frac{(\kappa_{\rm p} + \kappa_{\rm s})}{2}\left(H^2 + \frac{D^2}{2}[\cos(4\theta_{\rm pc}) + 1]\right) \\ &\quad - (\kappa_{\rm p} C_{\rm p} + \kappa_{\rm s} C_{\rm s})H + \frac{\kappa_{\rm p} C_{\rm p}^2 + \kappa_{\rm s} C_{\rm s}^2}{2} \\ &\quad + (\kappa_{\rm p} - \kappa_{\rm s})HD\cos(2\theta_{\rm pc}) \\ &\quad - (\kappa_{\rm p} C_{\rm p} - \kappa_{\rm s} C_{\rm s})D\cos(2\theta_{\rm pc})\Bigg], \quad (4) \end{aligned}$$

where $a_{\rm p}$ is the contact area of the bound protein, $\kappa_{\rm p}$ and $C_{\rm p}$ are the bending rigidity and spontaneous curvature along the protein axis, respectively, and $\kappa_{\rm s}$ and $C_{\rm s}$ are along the side axis. From the comparison of the experimental data of tethered vesicles [16,17], the bending rigidity and spontaneous curvature along the protein axis were estimated as $\kappa_{\rm p}/k_{\rm B}T = 82 \pm 20$ and $C_{\rm p}\ ({\rm nm}^{-1}) = -0.047 + 0.0003(\kappa_{\rm p}/k_{\rm B}T - 82) \pm 0.001$ for the I-BAR domain and $30 \lesssim \kappa_{\rm p}/k_{\rm B}T \lesssim 60$ and $0.06 \lesssim C_{\rm p}\ ({\rm nm}^{-1}) \lesssim 0.09$ for the N-BAR domain [37].

Different forms of the anisotropic bending energy have also been used. In Ref. [32] only the linear terms of H and D were considered in addition to the tilt energy. In Ref. [33] the energy was considered to be

$$\begin{aligned} U_{\rm grad} &= \frac{k_{\rm m}}{2}(H - H_0)^2 \\ &\quad + \frac{k_{\rm m} + k_{\rm d}}{4}\left[D^2 - 2DD_0\cos(2\theta_{\rm pc}) + D_0^2\right]. \quad (5) \end{aligned}$$

The second term assumes an energy proportional to a rotational average in the squared gradient of the normal curvature $C_\ell - C_p$ with respect to the protein rotation. In this form, the protein depends only weakly on the protein orientation; the cross term of HD does not appear and the D^2 term is independent of the angle $\theta_{\rm pc}$.

In these protein models, the bending energy depends on the angle only as a function of $\cos(2\theta_{\rm pc})$, owing to symmetry. For

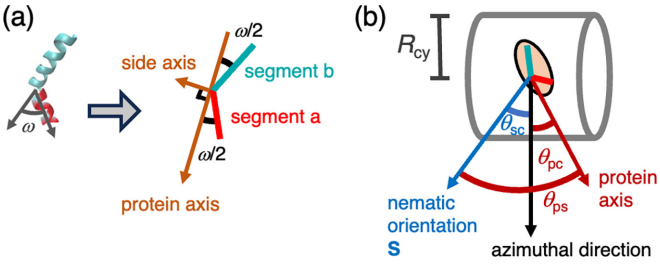

FIG. 2. Schematic of an asymmetric curvature-inducing protein. (a) Model of the protein with two rodlike segments. (b) Protein on a cylindrical membrane. The angles between the nematic direction **S**, azimuthal direction, and/or protein axis are depicted.

asymmetric proteins, the energy can include an odd function of the angle θ_{pc}. Such a term was previously considered in the model by Akabori and Santangelo [34]. They added the term

$$U_{asy} = k_{asy}[D\sin(2\theta_{pc}) - C_{asy}]^2 \tag{6}$$

to Eq. (3), where $D\sin(2\theta_{pc})$ is the nondiagonal element of the curvature tensor. In Ref. [58] this model was used to estimate the bending rigidities of amphipathic peptides. However, this model does not have a microscopic basis. In this study we examine the bending energies of asymmetric proteins using a two-rod protein model.

III. PROTEIN CONSISTING OF TWO RODS

A. Protein model

We consider a protein or peptide consisting of two segments [segments a and b in Fig. 2(a)]. Each segment is modeled as the symmetric protein model (in the absence of side bending rigidity for simplicity) and the orientations of the two segments have an angle ω on the membrane surface. Melittin is an example of this type of molecule, in which two α helices are connected by a kink. The bending energy of one protein is expressed as

$$\begin{aligned} U_{2rod} =& \frac{\kappa_{pa}a_{pa}}{2}(C_{\ell 1a} - C_{pa})^2 + \frac{\kappa_{pb}a_{pb}}{2}(C_{\ell 1b} - C_{pb})^2 \\ =& \kappa_{pm}a_p\Big((H - C_{pm})^2 + C_{pd}^2 + 2(H - C_{pm})D\cos(\omega)\cos(2\theta_{pc}) \\ &+ 2C_{pd}D\sin(\omega)\sin(2\theta_{pc}) + \frac{D^2}{2}[\cos(2\omega)\cos(4\theta_{pc}) + 1]\Big) \\ &+ \kappa_{pd}a_p\Big(- 2HC_{pd} + 2C_{pm}C_{pd} - 2C_{pd}D\cos(\omega)\cos(2\theta_{pc}) \\ &- 2(H - C_{pm})D\sin(\omega)\sin(2\theta_{pc}) - \frac{D^2}{2}\sin(2\omega)\sin(4\theta_{pc})\Big), \end{aligned} \tag{7}$$

where $C_{pm} = (C_{pa} + C_{pb})/2$, $C_{pd} = (C_{pa} - C_{pb})/2$, $\kappa_{pm}a_p = (\kappa_{pa}a_{pa} + \kappa_{pb}a_{pb})/2$, and $\kappa_{pd}a_p = (\kappa_{pa}a_{pa} - \kappa_{pb}a_{pb})/2$. We use $\kappa_{pm} = 50k_BT$ and $a_pC_{pm}^2 = 0.1$. These values are typical of curvature-inducing proteins. The angle $\omega = \pi/6$ is used unless specified otherwise. Note that κ_{pd} varies according to the bending rigidity difference and the area difference between the two segments.

In Eq. (7) the deviatoric curvature D and angle θ_{pc} always appear as pairs as a function of $D\cos(2\theta_{pc})$ and/or $D\sin(2\theta_{pc})$. The asymmetric terms proportional to $HD\sin(2\theta_{pc})$ and to $D^2\sin(4\theta_{pc})$ exist in addition to the term proportional to $D\sin(2\theta_{pc})$. Therefore, the asymmetric energy described in Eq. (6) [34] is insufficient to express the asymmetric bending energy.

For a symmetric protein ($C_{pd} = k_{pd} = 0$), the bending energy is expressed as

$$\begin{aligned} U_{2rod}^{sym} =& \frac{\kappa_{pm}a_p}{2}[1 + \cos(\omega)](C_{\ell 1} - C_{pm})^2 \\ &+ \frac{\kappa_{pm}a_p}{2}[1 - \cos(\omega)](C_{\ell 2} - C_{pm})^2 \\ &- \frac{\kappa_{pm}a_p}{2}D^2[1 - \cos(2\omega)]\cos(4\theta_{pc}). \end{aligned} \tag{8}$$

The first and second terms correspond to the bending energies along the main and side axes of the protein in Eq. (3), respectively. However, the last term is new. At $\omega = 0$, the second and last terms vanish, and with increasing ω, they increase.

B. Isolated proteins

First, we consider protein binding at the low-density limit, in which bound proteins are isolated on a membrane and interprotein interactions are negligible. Hence, the density ϕ of bound proteins is given by $\phi = (1/2\pi)\int_{-\pi}^{\pi}\exp[\beta(\mu - U_{2rod})]d\theta_{pc}$, where μ is the binding chemical potential and $\beta = 1/k_BT$. The binding ratio of proteins to a cylindrical membrane tube with respect to a flat membrane is expressed as

$$\frac{\phi_{cy}}{\phi_{flat}} = \frac{\exp(\beta U_{2rod}^{flat})}{2\pi}\int_{-\pi}^{\pi}\exp\big(-\beta U_{2rod}^{cy}\big)d\theta_{pc}, \tag{9}$$

where U_{2rod}^{flat} is the bending energy for the flat membrane ($H = D = 0$) and U_{2rod}^{cy} is that for the cylindrical membrane ($H = D = 1/2R_{cy}$). This ratio ϕ_{cy}/ϕ_{flat} is independent of μ at the low-density limit ($\phi_{cy} \ll 1$ and $\phi_{flat} \ll 1$).

Figure 3 shows the dependence on the curvature $1/R_{cy}$ of the cylindrical membrane for symmetrical proteins [Eq. (8)] with a fixed angle ω. The binding density reaches a maximum at $1/R_{cy}C_{pm} \simeq 1.2$, and the maximum level decreases with increasing ω. Hence, the preferred curvature of the protein is slightly higher than that of each segment, C_{pm}. The density distribution is mirror symmetric with respect to $\theta_{pc} = 0$ and has one or two peaks θ_{peak} at low or high membrane curvatures, respectively [see Fig. 3(b) and the dashed lines in Fig. 4(c)]. This peak split occurs since the membrane curvature becomes higher than the preferred curvature for the protein at high curvatures. Each protein segment has the lowest bending energy when it is along the azimuthal direction for $1/R_{cy}C_{pm} \leqslant 1$, whereas it deviates from the azimuthal direction as $\theta_{pc} \pm \omega/2 = \pm\arccos(\sqrt{R_{cy}C_{pm}})$ for $1/R_{cy}C_{pm} > 1$. For $\omega = \pi/6$, the split point is shifted to a slightly higher membrane curvature [see Fig. 3(b)], since two segments are tilted with $\pm\omega/2$, when the protein is oriented in the azimuthal direction ($\theta_{pc} = 0$). When the orthogonal protein model given in Eq. (3) is used, i.e., the last term in Eq. (8) is not

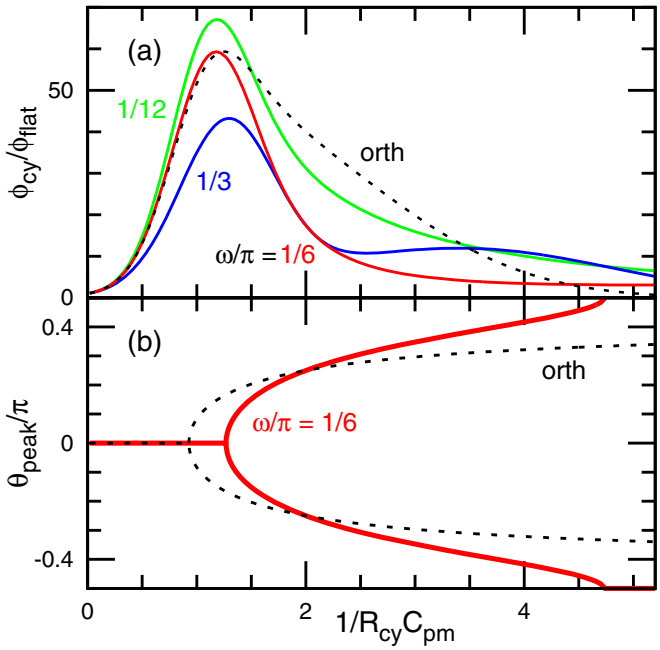

FIG. 3. Binding of symmetric proteins ($\kappa_{pd} = C_{pd} = 0$) at the low-density limit. (a) Binding density ϕ_{cy} on a cylindrical membrane with respect to the density ϕ_{flat} on a flat membrane. The solid lines represent the data for $\omega/\pi = 1/12$, $1/6$, and $1/3$ (from top to bottom in the left region, respectively). (b) Peak position of the angle θ_{pc} at $\omega/\pi = 1/6$. The dashed lines in both (a) and (b) represent the data obtained using the orthogonal approximation at $\omega/\pi = 1/6$.

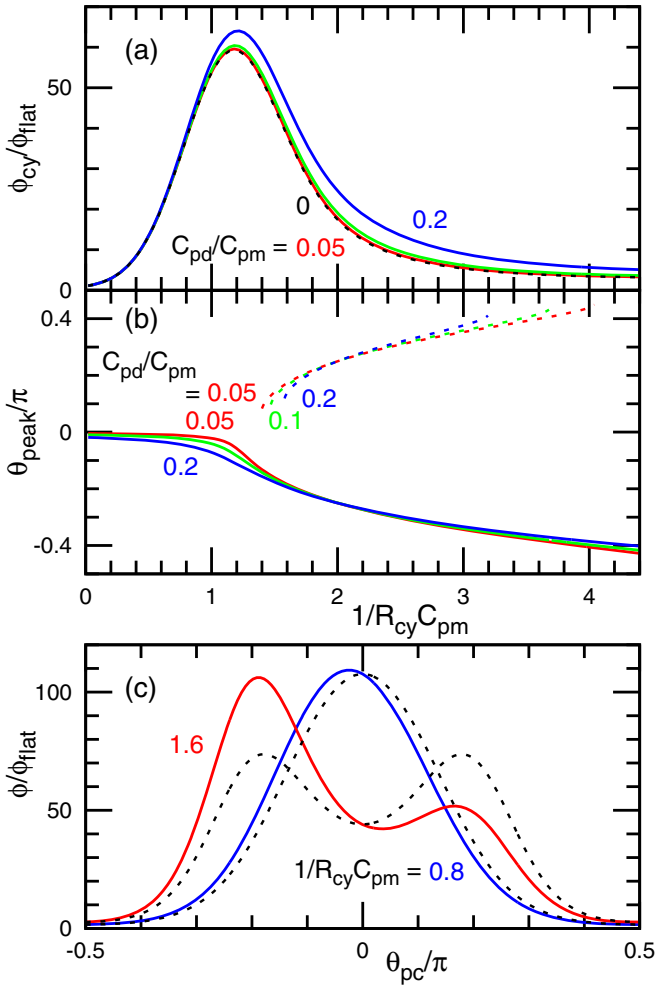

FIG. 4. Binding of asymmetric proteins with $\kappa_{pd} = 0$ and $\omega/\pi = 1/6$ at the low-density limit. (a) Binding density ϕ_{cy} on a cylindrical membrane with respect to the density ϕ_{flat} on a flat membrane. The solid lines represent the data at $C_{pd}/C_{pm} = 0.2$, 0.1, and 0.05 from top to bottom. The dashed line represents the data at $C_{pd} = 0$ (the symmetric condition). (b) Peak position of the angle θ_{pc}. The solid and dashed lines represent the first and second peaks, respectively. (c) Distribution of the angle θ_{pc} at $1/R_{cy}C_{pm} = 0.8$ and 1.6. The solid and dashed lines represent the data for $C_{pd}/C_{pm} = 0.1$ and 0, respectively.

accounted for, the protein behavior can be reproduced well at low membrane curvatures but not at high curvatures (see the dashed lines in Fig. 3). Therefore, the last term in Eq. (8) significantly modifies protein behavior at high membrane curvatures.

Next we consider the asymmetric proteins with $\omega = \pi/6$ (see Figs. 4 and 5). Figure 4 shows the case in which the spontaneous curvatures of two segments are different while keeping $\kappa_{pd} = 0$. Since segment a has a large spontaneous curvature, it is oriented more in the azimuthal direction than segment b. Hence, the peak angle of θ_{pc} becomes negative and decreases continuously with increasing $1/R_{cy}$ [see Fig. 4(b)]. The upper peak becomes the second maximum for a finite range of $1/R_{cy}$ [see the solid lines in Fig. 4(c)]. The width of this range decreases with increasing C_{pd} [see dashed lines in Fig. 4(b)]. However, the binding protein ratio ϕ_{cy}/ϕ_{flat} is only slightly modified [see Fig. 4(a)].

When the bending rigidities of the two segments are different, the proteins exhibit more complicated behavior. For a small curvature of $1/R_{cy}$, the angle distribution is slightly asymmetric and has a peak at $\theta_{pc} < 0$, as in the previous case [compare Figs. 4(c) and 5(c)]. However, the peak position shifts to $\theta_{pc} > 0$ with increasing $1/R_{cy}$ and a second peak appears at $\theta_{pc} < 0$. At $1/R_{cy}C_{pm} > 2$, the peak at $\theta_{pc} < 0$ becomes larger than the other one [see Figs. 5(b) and 5(c)]. These peak behaviors are caused by the last two terms in Eq. (7). The sign of the penultimate term changes at $1/R_{cy}C_{pm} = 2$, and the increase in θ_{peak} at $1/R_{cy}C_{pm} \simeq 1$ is mainly due to the last term.

When both the bending rigidities and spontaneous curvatures of the two segments are different, the ratio ϕ_{cy}/ϕ_{flat} can vary considerably from that of symmetric protein and the angle distribution can be more asymmetrical [see the uppermost line in Fig. 5(a) and the dashed line in Fig. 5(c)]. This increase in ϕ_{cy}/ϕ_{flat} is due to the enhancement of protein curvature induction by the effectively large protein curvature $[\kappa_{pa}a_{pa}C_{pa} + \kappa_{pb}a_{pb}C_{pb} = (\kappa_{pm}a_pC_{pm} + \kappa_{pd}a_pC_{pd})/2]$.

Further, we consider the conformational fluctuations in the protein. To allow an angle fluctuation of ω, a harmonic potential $U_\omega = (k_\omega k_B T/2)(\omega - \omega_0)^2$ is added, where $\omega_0 = \pi/6$. At $k_\omega = 0$, the two segments act as two separate rods, and the binding ratio ϕ_{cy}/ϕ_{flat} exhibits a smaller peak and broader tail, since the effective bending rigidity is smaller but the orientation is less constrained, respectively (see Fig. 6).

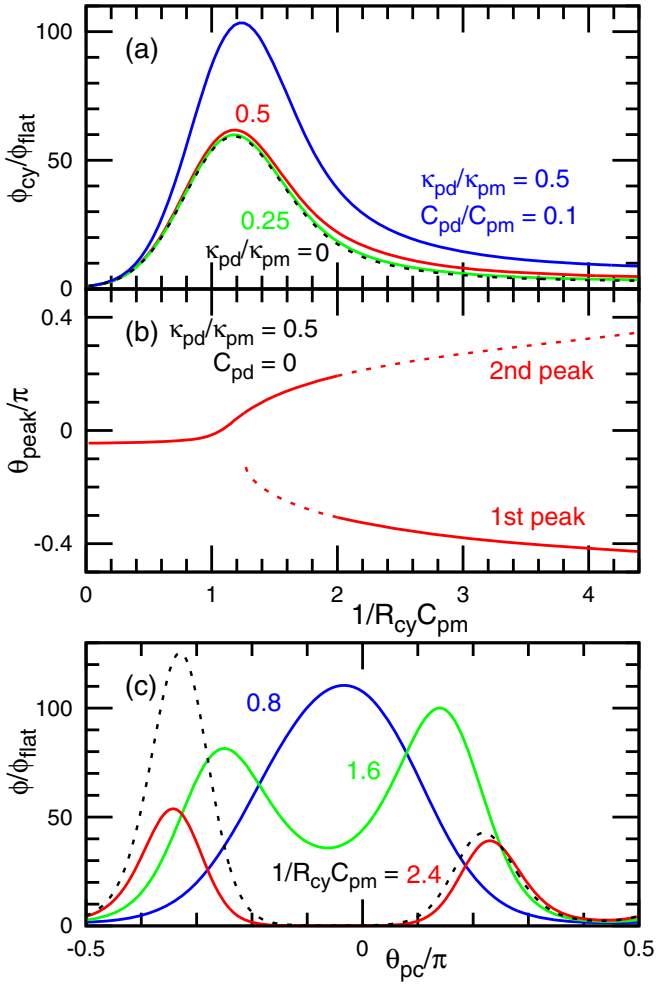

FIG. 5. Binding of asymmetric proteins with $\kappa_{pd} > 0$ and $\omega/\pi = 1/6$ at the low-density limit. (a) Binding density ϕ_{cy} on a cylindrical membrane with respect to the density ϕ_{flat} on a flat membrane. The uppermost line represents the data at $\kappa_{pd}/\kappa_{pm} = 0.5$ and $C_{pd}/C_{pm} = 0.1$. The lower two solid lines represent the data for $\kappa_{pd}/\kappa_{pm} = 0.5$ and 0.25 at $C_{pd} = 0$. The dashed line represents the data at $\kappa_{pd} = 0$ and $C_{pd} = 0$ (the symmetric condition). (b) Peak position of the angle θ_{pc} at $\kappa_{pd}/\kappa_{pm} = 0.5$ and $C_{pd} = 0$. The solid and dashed lines represent the first and second peaks, respectively. (c) Distribution of the angle θ_{pc} at $\kappa_{pd}/\kappa_{pm} = 0.5$. The solid lines represent the data for $1/R_{cy}C_{pm} = 0.8$, 1.6, and 2.4 at $C_{pd} = 0$. The dashed line represents the data at $1/R_{cy}C_{pm} = 2.4$ and $C_{pd}/C_{pm} = 0.1$.

As k_ω increases, the ratio continuously changes into that at the fixed angle.

C. Density dependence

As the binding density increases, interprotein interactions have more significant effects on protein binding. Here we use the mean-field theory [35–37], including orientation-dependent excluded-volume interactions based on the theory of Nascimento *et al.* for three-dimensional liquid crystals [69]. Although two-rod proteins likely form a smectic liquid crystal at high densities, we consider only the isotropic and nematic phases in this study.

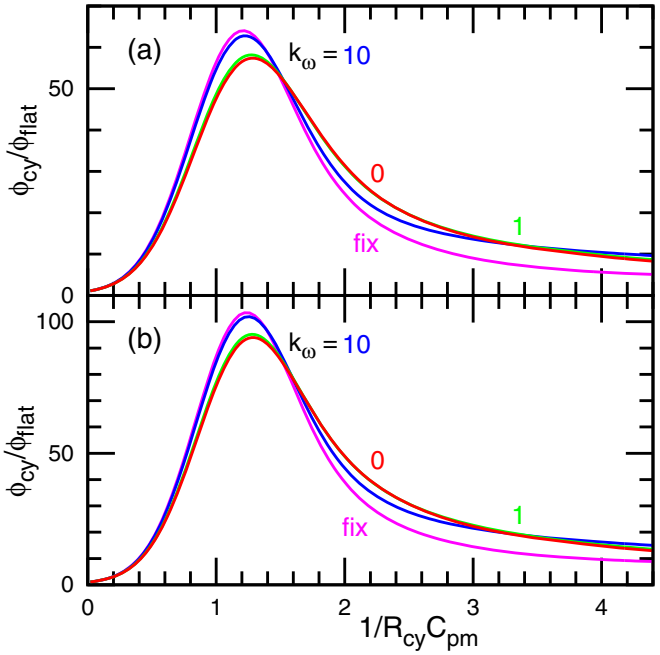

FIG. 6. Binding density of asymmetric proteins with the harmonic angle potential at the low-density limit and (a) $\kappa_{pd} = 0$ and $C_{pd}/C_{pm} = 0.2$ and (b) $\kappa_{pd}/\kappa_{pm} = 0.5$ and $C_{pd}/C_{pm} = 0.1$. The potential strength is varied as $k_\omega = 0$, 1, and 10 at $\omega_0/\pi = 1/6$. The lowest lines in the right region ($1/R_{cy}C_{pm} > 2$) represent the data when the angle is fixed at $\omega/\pi = 1/6$.

The free energy F_p of the bound proteins is expressed as

$$F_p = \int f_p dA, \tag{10}$$

$$f_p = \frac{\phi k_B T}{a_p}\left[\ln(\phi) + \frac{S\Psi}{2} - \ln\left(\int_{-\pi}^{\pi} w(\theta_{ps})d\theta_{ps}\right)\right], \tag{11}$$

$$w(\theta_{ps}) = g\exp\left(\Psi s_p(\theta_{ps}) + \bar{\Psi}\sin(\theta_{ps})\cos(\theta_{ps}) - \frac{U_{2rod}}{k_B T}\right)\Theta(g), \tag{12}$$

$$g = 1 - \phi[b_0 - b_2 S s_p(\theta_{ps})], \tag{13}$$

where $s_p(\theta_{ps}) = \cos^2(\theta_{ps}) - 1/2$ and $\Theta(x)$ denotes the unit step function. The order of proteins is obtained by an ensemble average (denoted by angular brackets) of $2s_p$:

$$S = 2\langle s_p(\theta_{ps})\rangle \tag{14}$$

$$= 2\frac{\int_{-\pi}^{\pi} s_p(\theta_{ps})w(\theta_{ps})d\theta_{ps}}{\int_{-\pi}^{\pi} w(\theta_{ps})d\theta_{ps}}, \tag{15}$$

where θ_{ps} denotes the angle between the major protein axis and ordered direction **S** (see Fig. 2). The factor g expresses the effect of the orientation-dependent excluded volume, where $b_0 = (4 + b_{exc}/2)\lambda$ and $b_2 = b_{exc}\lambda$. Here we use $\lambda = 1/3$ and $b_{exc} = 1.98$ for an elliptic protein with an aspect ratio of $\ell_1/\ell_2 = 3$, where ℓ_1 and ℓ_2 are the lengths in the major and minor axes, respectively [36]. Proteins can have nonoverlapping conformations at $g > 0$ and hence the maximum density is given by a function of S as $\phi_{lim}(S) = 1/(b_0 - b_2 S/2)$ [see the rightmost line in Fig. 7(b)]. The quantities Ψ and

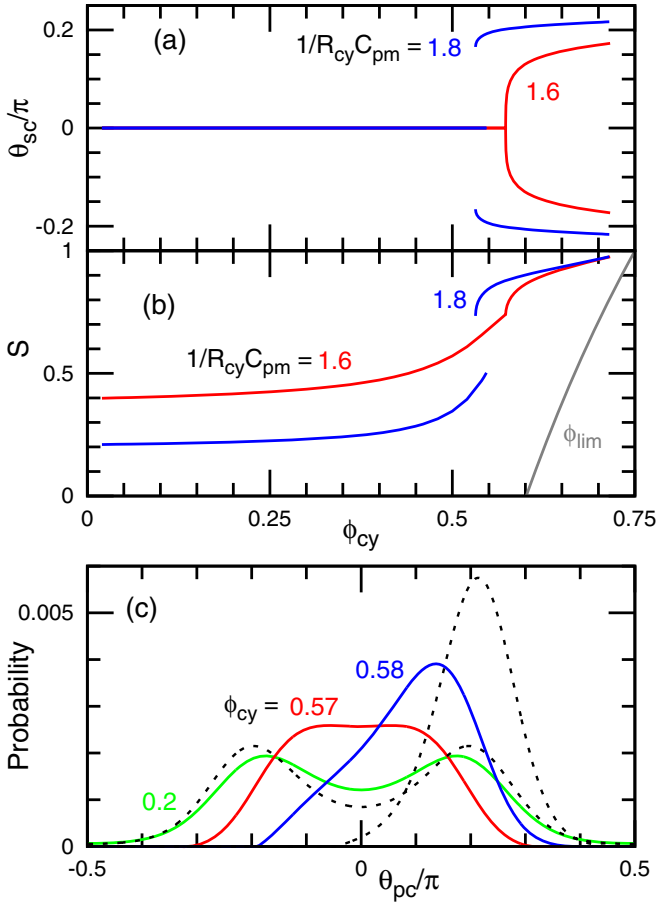

FIG. 7. Binding of symmetric proteins ($\kappa_{pd} = C_{pd} = 0$) for finite densities ϕ_{cy} at $\omega/\pi = 1/6$. The second- and first-order transitions occur at $1/R_{cy}C_{pm} = 1.6$ and 1.8, respectively. (a) Angle θ_{sc} between the orientational order and azimuthal direction. (b) Orientational degree S of the proteins. The slanted gray line on the right represents the maximum density $\phi_{lim}(S)$. (c) Distribution of the angle θ_{pc}. The solid lines represent the data for $\phi_{cy} = 0.2$, 0.57, and 0.58 at $1/R_{cy}C_{pm} = 1.6$. The dashed lines represent the data for $\phi_{cy} = 0.5$ and 0.6 at $1/R_{cy}C_{pm} = 1.8$.

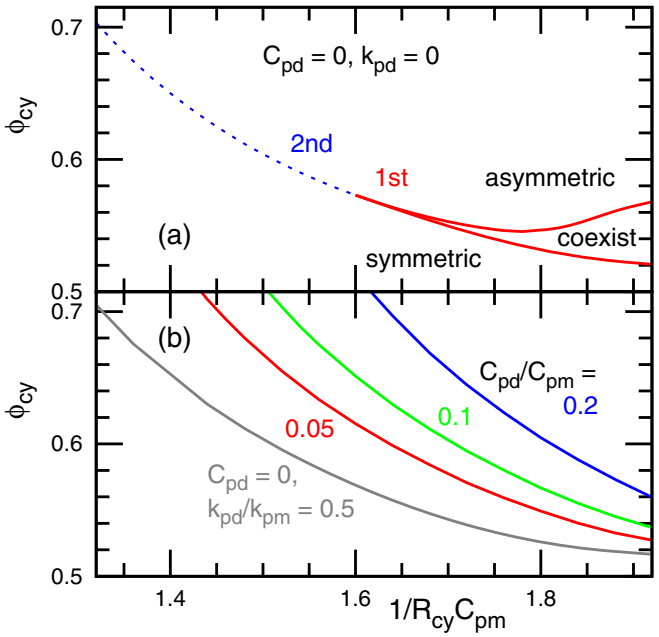

FIG. 8. Phase diagram for (a) symmetric proteins and (b) asymmetric proteins. (a) The dashed line represents the phase boundary of the second-order transition. The proteins exhibit symmetric and asymmetric distributions with respect to $\theta_{sc} = 0$ below and above the lines, respectively. Two states coexist between the two solid lines. (b) Boundaries of the metastable states. The upper three lines represent the data for $C_{pd}/C_{pm} = 0.2$, 0.1, and 0.05 at $\kappa_{pd} = 0$, from top to bottom. The lowest line represents the data for $\kappa_{pd}/\kappa_{pm} = 0.5$ and $C_{pd} = 0$.

$\bar{\Psi}$ are the symmetric and asymmetric components of the nematic tensor, respectively, and are determined using Eq. (15) and $\langle \sin(\theta_{ps})\cos(\theta_{ps})\rangle = 0$. Further details of this theory are described in Refs. [35,36].

For the symmetric proteins ($\kappa_{pd} = C_{pd} = 0$), the density dependence is qualitatively the same as that for the one-rod proteins ($\omega = 0$) reported in Ref. [36]. On a cylindrical membrane with a small curvature of $1/R_{cy}C_{pm} \lesssim 0.2$, the two-rod proteins with $\omega = \pi/6$ exhibit an isotropic-nematic transition at $\phi_{cy} \simeq 0.11$ (data not shown). At a middle curvature $0.2 \lesssim 1/R_{cy}C_{pm} \leqslant 1$, the proteins exhibit no phase transition and the orientational order S increases continuously with increasing ϕ_{cy} (data not shown). At $1/R_{cy}C_{pm} < 1$, the preferred direction of the proteins is the azimuthal direction of the membrane tube, i.e., $\theta_{sc} = 0$. At $1/R_{cy}C_{pm} \gtrsim 1.3$, the preferred direction is tilted symmetrically to the positive and negative angles, as previously explained (see Fig. 3). At low densities, proteins with positive and negative preferred angles can coexist at the same amount with keeping $\theta_{sc} = 0$. In contrast, at high densities, this coexistence is prevented by the larger excluded-volume interactions between proteins of the different angles. Second- and first-order phase transitions occur between these two states for middle membrane curvatures ($1/R_{cy}C_{pm} < 1.6$) and high membrane curvatures ($1/R_{cy}C_{pm} > 1.6$), respectively [see Figs. 7 and 8(a)]. At the first-order transition, the distribution of θ_{pc} changes from two symmetrical peaks to either peak [see the dashed lines in Fig. 7(c)] and θ_{sc} and S exhibit discrete changes [see Figs. 7(a) and 7(b)]. Conversely, for the second-order transition, the two peaks are pushed to $\theta_{pc} = 0$ and unified to reduce the excluded volume before the transition, following which the single peak continuously moves into either the positive or the negative direction above the transition point [see the solid lines in Fig. 7(c)]. In the phase diagram, the curves of the second- and first-order transitions meet at a single point as shown in Fig. 8(a). A similar phase diagram is obtained for the one-rod proteins ($\omega = 0$).

For the asymmetric proteins ($\kappa_{pd} \neq 0$ or $C_{pd} \neq 0$), the transition becomes a continuous change; however, a metastable state appears at a high density (see Figs. 9 and 10). At $\kappa_{pd} = 0$ and $C_{pd} > 0$, the negative angles of θ_{pc} have lower bending energies [see Fig. 4(c)] such that the branch of $\theta_{sc} < 0$ becomes the equilibrium state (see Fig. 9). The other branch becomes the metastable state that appears at higher membrane curvatures and the lower-bound curvature increases with increasing C_{pd} [see Fig. 8(b)]. Interestingly, at $\kappa_{pd}/\kappa_{pm} = 0.5$ and $C_{pd} = 0$, the equilibrium value of θ_{sc} changes the sign

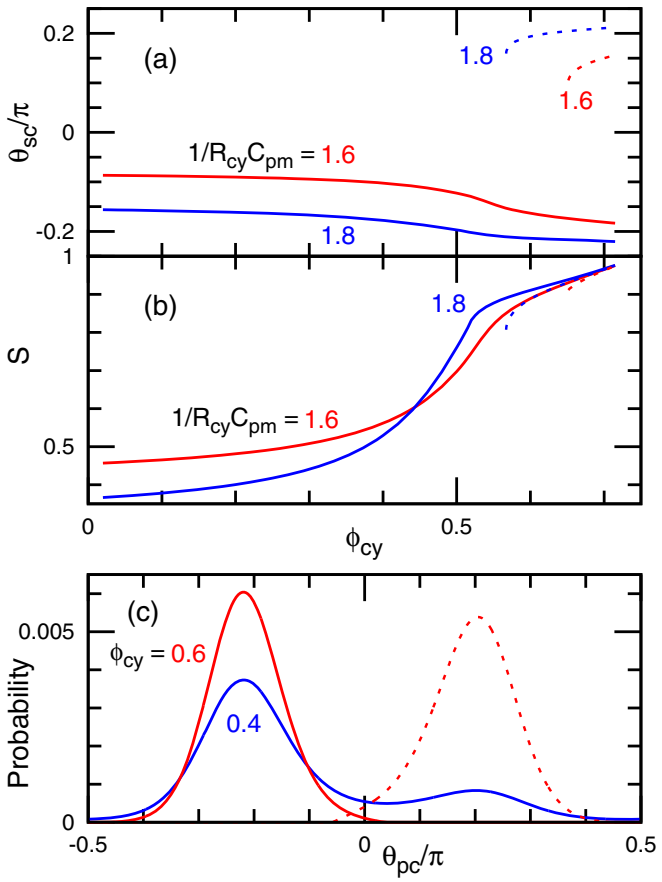

FIG. 9. Binding of asymmetric proteins with $C_{\rm pd}/C_{\rm pm} = 0.1$, $\kappa_{\rm pd} = 0$, and $\omega/\pi = 1/6$ at finite densities $\phi_{\rm cy}$. (a) Angle $\theta_{\rm sc}$ between the orientational order and azimuthal direction at $1/R_{\rm cy}C_{\rm pm} = 1.6$ and 1.8. (b) Orientational degree S of the proteins at $1/R_{\rm cy}C_{\rm pm} = 1.6$ and 1.8. (c) Distribution of the angle $\theta_{\rm pc}$ for $\phi_{\rm cy} = 0.4$ and 0.6 at $1/R_{\rm cy}C_{\rm pm} = 1.8$. The solid and dashed lines represent the equilibrium and metastable states, respectively.

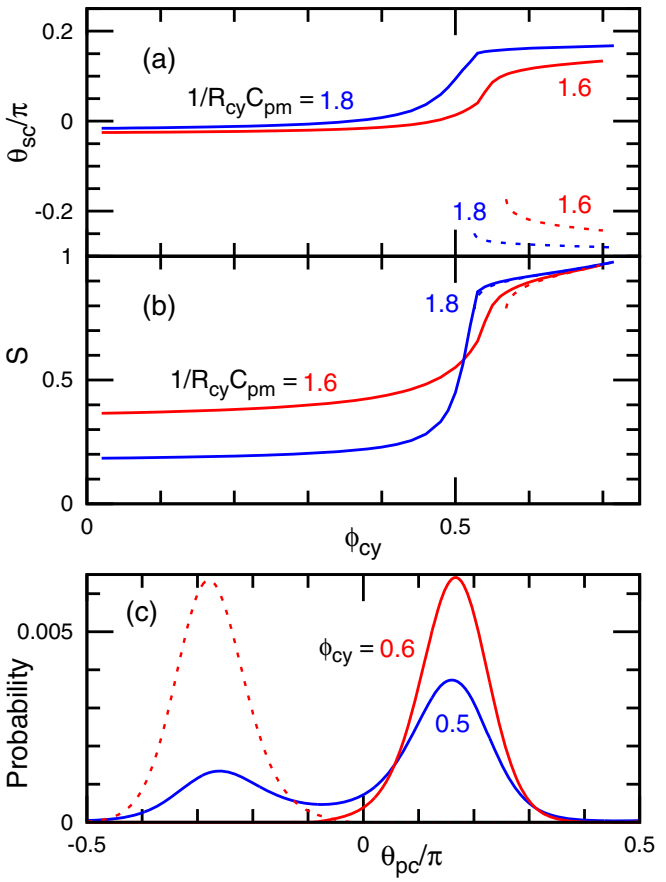

FIG. 10. Binding of asymmetric proteins with $\kappa_{\rm pd}/\kappa_{\rm pm} = 0.5$, $C_{\rm pd} = 0$, and $\omega/\pi = 1/6$ at finite densities $\phi_{\rm cy}$. (a) Angle $\theta_{\rm sc}$ between the orientational order and azimuthal direction at $1/R_{\rm cy}C_{\rm pm} = 1.6$ and 1.8. (b) Orientational degree S of the proteins at $1/R_{\rm cy}C_{\rm pm} = 1.6$ and 1.8. (c) Distribution of the angle $\theta_{\rm pc}$ for $\phi_{\rm cy} = 0.5$ and 0.6 at $1/R_{\rm cy}C_{\rm pm} = 1.8$. The solid and dashed lines represent the equilibrium and metastable states, respectively.

with increasing $\phi_{\rm cy}$ [see Fig. 10(a)]. This is due to high and low peaks at $\theta_{\rm pc} = \theta_1$ and $-\theta_2$ with $0 < \theta_1 < \theta_2$ [see the middle solid line in Fig. 5(c)]. With increasing $\phi_{\rm cy}$, the lower peak is reduced and subsequently disappears in the equilibrium state [see the solid lines in Fig. 10(c)]. Thus, the asymmetry of proteins causes the transition to become a continuous change. It resembles the aforementioned change from the first order to continuous change at $1/R_{\rm cy}C_{\rm pm} \simeq 0.2$ in the symmetric proteins. Note that taking a different protein axis for the elliptical approximation does not change this binding behavior except for the protein angles. When the axis of segment a is taken, the values of $\theta_{\rm sc}$ and $\theta_{\rm pc}$ are shifted by $\omega/2$, while S is unchanged.

IV. PROTEINS OF THREEFOLD OR HIGHER ROTATIONAL SYMMETRY

Single proteins or protein assemblies often exhibit N-fold rotational symmetry with $N \geqslant 3$. First, we consider cases with perfect rotational symmetry. The bending energy of an N-fold rotationally symmetric protein is generically expressed as

$$U_{{\rm r},N}(H, K, D, \theta_{\rm p1}) = \sum_{j=1}^{N} u_0\Big(H, K, D\cos\Big[2\Big(\theta_{\rm p1} + \frac{2\pi j}{N}\Big)\Big], D \times \sin\Big[2\Big(\theta_{\rm p1} + \frac{2\pi j}{N}\Big)\Big]\Big), \tag{16}$$

where $K = C_1C_2$ is the Gaussian curvature, $u_0(H, K, D\cos[2(\theta_{\rm p1} + 2\pi j/N)], D\sin[2(\theta_{\rm p1} + 2\pi j/N)])$ is the bending energy of the jth segment (or protein), and $\theta_{\rm p1}$ is the angle between the axis of the first segment and the direction of either principal membrane curvature. Here we consider only the linear and squared terms, as is usual for bending energies. For the symmetry, $U_{{\rm r},N}(H, K, D, \theta + 2\pi/N) = U_{{\rm r},N}(H, K, D, \theta)$. To satisfy this relation, the linear terms (proportional to $\cos[2(\theta_{\rm p1} + \frac{2\pi j}{N})]$ and $\sin[2(\theta_{\rm p1} + \frac{2\pi j}{N})]$) vanish for $N \geqslant 3$. The squared terms (proportional to $\cos[4(\theta_{\rm p1} + \frac{2\pi j}{N})]$ and $\sin[4(\theta_{\rm p1} + \frac{2\pi j}{N})]$) vanish for $N = 3$ and $N \geqslant 5$, because $e^{8\pi {\rm i}/N} = 1$ is satisfied at $N = 1$, 2, and 4 but otherwise not. Therefore, for the rotational symmetry of $N = 3$ and

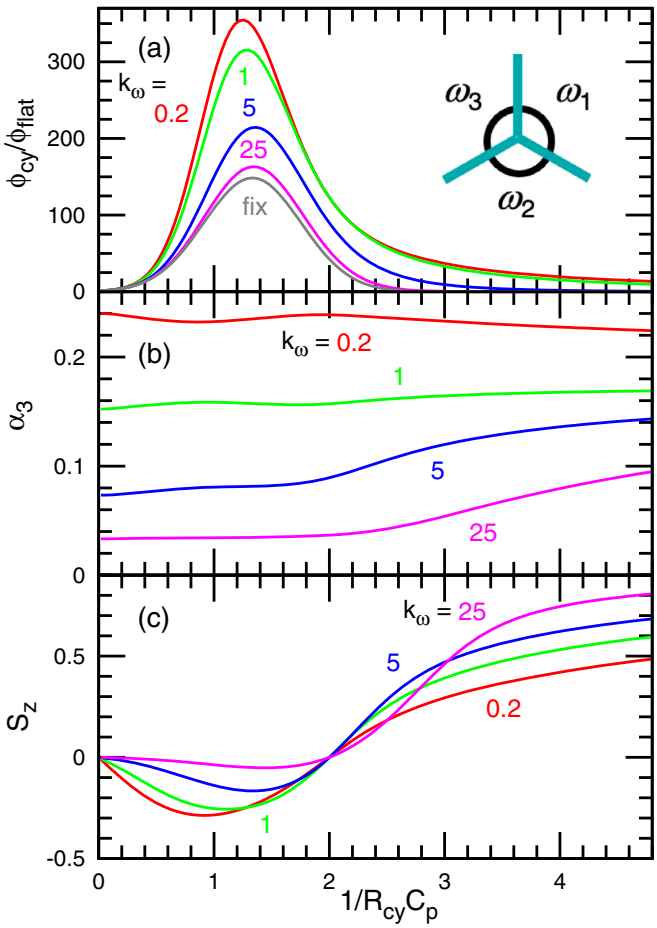

FIG. 11. Binding of threefold rotationally symmetric proteins at the low-density limit. (a) Binding density ϕ_{cy} on a cylindrical membrane with respect to the density ϕ_{flat} on a flat membrane. The upper four lines represent $k_\omega = 0.2$, 1, 5, and 25, from top to bottom. For the lowest line the angles are fixed as $\omega_1 = \omega_2 = \omega_3 = 2\pi/3$. The schematic of the protein is shown in the inset. (b) Deformation degree α_3 for $k_\omega = 0.2$, 1, 5, and 25. (c) Orientational degree S_z along the (z) axis of membrane tube for $k_\omega = 0.2$, 1, 5, and 25.

$N \geqslant 5$, the bending energy is independent of θ_{p1} but is a function of H and K, since $D^2 = H^2 - K$. Hence, it is laterally isotropic and the Canham-Helfrich energy [26,27] is applicable. For $N = 4$, the θ_{p1}-dependent term remains. When $u_0 = (\kappa_p a_p/2)\{H + D\cos[2(\theta_{p1} + \frac{2\pi j}{N})] - C_p\}^2$ is used, the protein bending energy is given by $U_{r,4}(H, K, D, \theta_{p1}) = \kappa_p a_p\{2H^2 + D^2[\cos(4\theta_{p1}) + 1] + 2C_p^2\}$.

Even when a protein has rotational symmetry in its native structure, the proteins can take asymmetric shapes under protein deformation. We consider a protein with threefold rotational symmetry, as shown in the inset of Fig. 11(a). Three crescent-rodlike segments are connected at the branching point with harmonic angle potentials

$$U_{3rod} = \sum_{j=1}^{3} \frac{\kappa_p a_p}{2}\left\{H + D\cos\left[2\left(\theta_{p1} + \frac{2\pi j}{N}\right)\right] - C_p\right\}^2 + \frac{k_\omega k_B T}{2}\left(\omega_j - \frac{2\pi}{3}\right)^2, \quad (17)$$

where ω_j is the angle between neighboring segments. We use $\kappa_p = 50 k_B T$ and $a_p C_p^2 = 0.1$. The protein deformation is quantified by a shape parameter $\alpha_3 = \sqrt{\langle (r_G/\ell_p)^2\rangle}$, where r_G is the distance between the center of mass and branching point of the protein and ℓ_p is the length of each protein segment. The orientational order S_z along the (z) axis of the membrane tube is given by $S_z = 2(z_G/r_G)^2 - 1$, where z_G is the z component of the center of mass of the protein (the branching point is the origin of the coordinate).

As the coefficient k_ω of the angle potentials decreases, the protein exhibits a larger deformation [see Fig. 11(b)] so that each segment can take its preferred orientation more frequently. Thus, the binding ratio ϕ_{cy}/ϕ_{flat} increases with decreasing k_ω [see Fig. 11(a)]. The deformed protein is oriented along the azimuthal and tube axes at low and high membrane curvatures, respectively [see Fig. 11(c)]. Therefore, protein deformation can induce anisotropic bending energy in rotationally symmetric proteins and enhance curvature sensing.

V. SUMMARY

We have studied curvature sensing of proteins with asymmetric shapes and/or protein deformation. Protein asymmetry breaks the symmetry of sensing with respect to the azimuthal direction on cylindrical membranes such that the transition between the symmetrical and asymmetrical angle distributions disappears and the other branch becomes a metastable state. The N-fold rotationally symmetric proteins with $N = 3$ or $N \geqslant 5$ exhibit laterally isotropic bending energies when the protein deformation is negligible. However, their deformation can generate asymmetry in the protein shape and enhance protein binding to membranes with preferred curvatures.

In this study we considered the proteins consisting of two rods as asymmetric proteins. The internal structures affect the curvature sensing at membrane curvatures higher than their preferred curvatures, whereas only small modifications occur at lower curvatures. In general, proteins can have more complicated internal structures. Hence, the protein bending energy can have nine independent coefficients in Eq. (7) as

$$\begin{aligned} U_{cv} = {} & k_1 H^2 + k_2 H + k_3 K + k_4 D\cos(2\theta_{pc}) \\ & + k_5 HD\cos(2\theta_{pc}) + k_6 D^2\cos(4\theta_{pc}) \\ & + k_7 D\sin(2\theta_{pc}) + k_8 HD\sin(2\theta_{pc}) + k_9 D^2\sin(4\theta_{pc}). \end{aligned} \quad (18)$$

Note that the constant term is neglected, since it can be included in the binding chemical potential as $\mu' = \mu + \mu_{cv}$. Isotropic proteins can have the first three terms ($k_1 = 2\kappa$, $k_2 = -2\kappa C_0$, and $k_3 = \bar{\kappa}$ in the Helfrich model [27]). Twofold rotationally or mirror symmetric proteins can have the first six terms (k_1–k_6) and asymmetric proteins can have all terms. However, it is difficult to determine so many parameters. The number of parameters should practically be reduced based on each protein structure and experimental or simulation data.

The asymmetry of the protein bending energy can be determined from the asymmetric angle distribution of bound proteins on symmetrically curved membranes, such as a

cylindrical tube. Currently, it is difficult to measure experimentally. However, for atomistic and coarse-grained molecular simulations, binding of a single protein is relatively easy to investigate. The angle distribution of the protein axis on cylindrical or buckled membranes [70,71] and the curvature sensing of proteins can be evaluated. A few types of proteins and peptides (amphipathic peptides [58] and F-BAR protein Pacsin1 [72]) have been investigated only on buckled membranes of a single membrane shape. Protein bending properties can be more quantitatively evaluated using membranes with various curvatures. In highly buckled membranes, the membrane curvature under the proteins can vary along the protein axis. This local curvature difference can also modify curvature sensing. These protein properties are important for a quantitative understanding of curvature sensing and generation. Although we focused on the curvature sensing in this study, the curvature generation should also be modified by the protein asymmetry.

ACKNOWLEDGMENT

This work was supported by JSPS KAKENHI Grant No. JP21K03481.

[1] H. T. McMahon and J. L. Gallop, Nature (London) **438**, 590 (2005).
[2] S. Suetsugu, S. Kurisu, and T. Takenawa, Physiol. Rev. **94**, 1219 (2014).
[3] L. Johannes, R. G. Parton, P. Bassereau, and S. Mayor, Nat. Rev. Mol. Cell Biol. **16**, 311 (2015).
[4] T. Itoh and P. De Camilli, Biochim. Biophys. Acta **1761**, 897 (2006).
[5] M. Masuda and N. Mochizuki, Semin. Cell Dev. Biol. **21**, 391 (2010).
[6] C. Mim and V. M. Unger, Trends Biochem. Sci. **37**, 526 (2012).
[7] A. Frost, R. Perera, A. Roux, K. Spasov, O. Destaing, E. H. Egelman, P. De Camilli, and V. M. Unger, Cell **132**, 807 (2008).
[8] J. H. Hurley, E. Boura, L.-A. Carlson, and B. Różycki, Cell **143**, 875 (2010).
[9] H. T. McMahon and E. Boucrot, Nat. Rev. Mol. Cell Biol. **12**, 517 (2011).
[10] F. Brandizzi and C. Barlowe, Nat. Rev. Mol. Cell Biol. **14**, 382 (2013).
[11] M. Mettlen, P.-H. Chen, S. Srinivasan, G. Danuser, and S. L. Schmid, Annu. Rev. Biochem. **87**, 871 (2018).
[12] R. J. Taylor, G. Tagiltsev, and J. A. G. Briggs, FEBS Lett. **597**, 819 (2023).
[13] T. Baumgart, B. R. Capraro, C. Zhu, and S. L. Das, Annu. Rev. Phys. Chem. **62**, 483 (2011).
[14] C. Has and S. L. Das, Biochim. Biophys. Acta **1865**, 129971 (2021).
[15] B. Sorre, A. Callan-Jones, J. Manzi, B. Goud, J. Prost, P. Bassereau, and A. Roux, Proc. Natl. Acad. Sci. USA **109**, 173 (2012).
[16] C. Prévost, H. Zhao, J. Manzi, E. Lemichez, P. Lappalainen, A. Callan-Jones, and P. Bassereau, Nat. Commun. **6**, 8529 (2015).
[17] F.-C. Tsai, M. Simunovic, B. Sorre, A. Bertin, J. Manzi, A. Callan-Jones, and P. Bassereau, Soft Matter **17**, 4254 (2021).
[18] A. Roux, G. Koster, M. Lenz, B. Sorre, J.-B. Manneville, P. Nassoy, and P. Bassereau, Proc. Natl. Acad. Sci. USA **107**, 4141 (2010).
[19] G. Moreno-Pescador, C. D. Florentsen, H. Østbye, S. L. Sønder, T. L. Boye, E. L. Veje, A. K. Sonne, S. Semsey, J. Nylandsted, R. Daniels, and P. M. Bendix, ACS Nano **13**, 6689 (2019).
[20] K. R. Rosholm, N. Leijnse, A. Mantsiou, V. Tkach, S. L. Pedersen, V. F. Wirth, L. B. Oddershede, K. J. Jensen, K. L. Martinez, N. S. Hatzakis, P. M. Bendix, A. Callan-Jones, and D. Stamou, Nat. Chem. Biol. **13**, 724 (2017).
[21] S. Aimon, A. Callan-Jones, A. Berthaud, M. Pinot, G. E. S. Toombes, and P. Bassereau, Dev. Cell **28**, 212 (2014).
[22] S. Yang, X. Miao, S. Arnold, B. Li, A. T. Ly, H. Wang, M. Wang, X. Guo, M. Pathak, W. Zhao, C. D. Cox, and Z. Shi, Nat. Commun. **13**, 7467 (2022).
[23] J. B. Larsen, K. R. Rosholm, C. Kennard, S. L. Pedersen, H. K. Munch, V. Tkach, J. J. Sakon, T. Bjørnholm, K. R. Weninger, P. M. Bendix, K. J. Jensen, N. S. Hatzakis, M. J. Uline, and D. Stamou, ACS Cent. Sci. **6**, 1159 (2020).
[24] N. S. Hatzakis, V. K. Bhatia, J. Larsen, K. L. Madsen, P.-Y. Bolinger, A. H. Kunding, J. Castillo, U. Gether, P. Hedegård, and D. Stamou, Nat. Chem. Biol. **5**, 835 (2009).
[25] W. F. Zeno, W. T. Snead, A. S. Thatte, and J. C. Stachowiak, Soft Matter **15**, 8706 (2019).
[26] P. B. Canham, J. Theor. Biol. **26**, 61 (1970).
[27] W. Helfrich, Z. Naturforsch. **28**, 693 (1973).
[28] H. Noguchi, Int. J. Mod. Phys. B **36**, 2230002 (2022).
[29] Q. Goutaland, F. van Wijland, J.-B. Fournier, and H. Noguchi, Soft Matter **17**, 5560 (2021).
[30] H. Noguchi, Phys. Rev. E **104**, 014410 (2021).
[31] H. Noguchi, Soft Matter **17**, 10469 (2021).
[32] J.-B. Fournier, Phys. Rev. Lett. **76**, 4436 (1996).
[33] V. Kralj-Iglič, V. Heinrich, S. Svetina, and B. Žekš, Eur. Phys. J. B **10**, 5 (1999).
[34] K. Akabori and C. D. Santangelo, Phys. Rev. E **84**, 061909 (2011).
[35] C. Tozzi, N. Walani, A.-L. L. Roux, P. Roca-Cusachs, and M. Arroyo, Soft Matter **17**, 3367 (2021).
[36] H. Noguchi, C. Tozzi, and M. Arroyo, Soft Matter **18**, 3384 (2022).
[37] H. Noguchi, N. Walani, and M. Arroyo, Soft Matter **19**, 5300 (2023).
[38] H. Noguchi, Sci. Rep. **9**, 11721 (2019).
[39] N. Pietrosemoli, R. Pancsa, and P. Tompa, PLoS Comput. Biol. **9**, e1003144 (2013).
[40] D. J. Busch, J. R. Houser, C. C. Hayden, M. B. Sherman, E. M. Lafer, and J. C. Stachowiak, Nat. Commun. **6**, 7875 (2015).
[41] W. T. Snead, W. F. Zeno, G. Kago, R. W. Perkins, J. B. Richter, C. Zhao, E. M. Lafer, and J. C. Stachowiak, J. Cell Biol. **218**, 664 (2019).
[42] C. Hiergeist and R. Lipowsky, J. Phys. II (France) **6**, 1465 (1996).
[43] T. Bickel, C. Jeppesen, and C. M. Marques, Eur. Phys. J. E **4**, 33 (2001).

[44] T. Auth and G. Gompper, Phys. Rev. E **68**, 051801 (2003).
[45] T. Auth and G. Gompper, Phys. Rev. E **72**, 031904 (2005).
[46] H. Wu, H. Shiba, and H. Noguchi, Soft Matter **9**, 9907 (2013).
[47] D. Marsh, R. Bartucci, and L. Sportelli, Biochim. Biophys. Acta **1615**, 33 (2003).
[48] A. R. Evans, M. S. Turner, and P. Sens, Phys. Rev. E **67**, 041907 (2003).
[49] M. Werner and J.-U. Sommer, Eur. Phys. J. E **31**, 383 (2010).
[50] H. Noguchi, J. Chem. Phys. **157**, 034901 (2022).
[51] S. M. Ferguson and P. D. Camilli, Nat. Rev. Mol. Cell Biol. **13**, 75 (2012).
[52] B. Antonny, C. Burd, P. D. Camilli, E. Chen, O. Daumke, K. Faelber, M. Ford, V. A. Frolov, A. Frost, J. E. Hinshaw, T. Kirchhausen, M. M. Kozlov, M. Lenz, H. H. Low, H. McMahon, C. Merrifield, T. D. Pollard, P. J. Robinson, A. Roux, and S. Schmid, EMBO J. **35**, 2270 (2016).
[53] M. Pannuzzo, Z. A. McDargh, and M. Deserno, eLife **7**, e39441 (2018).
[54] H. Sato and J. B. Feix, Biochim. Biophys. Acta **1758**, 1245 (2006).
[55] I. Rady, I. A. Siddiqui, M. Rady, and H. Mukhtar, Cancer Lett. **402**, 16 (2017).
[56] S. Guha, J. Ghimire, E. Wu, and W. C. Wimley, Chem. Rev. **119**, 6040 (2019).
[57] Y. Miyazaki and W. Shinoda, Biochim. Biophys. Acta **1864**, 183955 (2022).
[58] J. Gómez-Llobregat, F. Elías-Wolff, and M. Lindén, Biophys. J. **110**, 197 (2016).
[59] S. F. Traynelis, L. P. Wollmuth, C. J. McBain, F. S. Menniti, K. M. Vance, K. K. Ogden, K. B. Hansen, H. Yuan, S. J. Myers, and R. Dingledine, Pharmacol. Rev. **62**, 405 (2010).
[60] J. Syrjanen, K. Michalski, T. Kawate, and H. Furukawa, J. Mol. Biol. **433**, 166994 (2021).
[61] O. P. Ernst, D. T. Lodowski, M. Elstner, P. Hegemann, L. S. Brown, and H. Kandori, Chem. Rev. **114**, 126 (2014).
[62] T. Nagata and K. Inoue, J. Cell Sci. **134**, jcs258989 (2021).
[63] A. J. Venkatakrishnan, X. Deupi, G. Lebon, C. G. Tate, G. F. Schertler, and M. M. Babu, Nature (London) **494**, 185 (2013).
[64] M. Shibata, K. Inoue, K. Ikeda, M. Konno, M. Singh, C. Kataoka, R. Abe-Yoshizumi, H. Kandori, and T. Uchihashi, Sci. Rep. **8**, 8262 (2018).
[65] V. Gerke, C. E. Creutz, and S. E. Moss, Nat. Rev. Mol. Cell Biol. **6**, 449 (2005).
[66] F. Oling, J. S. de Oliveira Santos, N. Govorukhina, C. Mazères-Dubut, W. Bergsma-Schutter, G. Oostergetel, W. Keegstra, O. Lambert, A. Lewit-Bentley, and A. Brisson, J. Mol. Biol. **304**, 561 (2000).
[67] C. D. Alas and C. A. Haselwandter, Phys. Rev. E **107**, 024403 (2023).
[68] H. Noguchi, Sci. Rep. **6**, 20935 (2016).
[69] E. S. Nascimento, P. Palffy-Muhoray, J. M. Taylor, E. G. Virga, and X. Zheng, Phys. Rev. E **96**, 022704 (2017).
[70] H. Noguchi, Phys. Rev. E **83**, 061919 (2011).
[71] M. Hu, P. Diggins IV, and M. Deserno, J. Chem. Phys. **138**, 214110 (2013).
[72] M. I. Mahmood, H. Noguchi, and K.-I. Okazaki, Sci. Rep. **9**, 14557 (2019).